

# Magnetostructural effects and phase transition in $\text{Cr}_2\text{O}_3$ under pressure

Alexander Yu. Dobin, Wenhui Duan, and Renata M. Wentzcovitch

*Department of Chemical Engineering and Material Sciences, School of Physics and Astronomy,  
and Minnesota Supercomputer Institute, University of Minnesota, Minneapolis, MN 55455*  
(October 27, 2018)

We have successfully calculated the electronic and structural properties of chromia ( $\text{Cr}_2\text{O}_3$ ) in the Local Spin Density Approximation (LSDA). We predict a transformation from the corundum to the  $\text{Rh}_2\text{O}_3$  (II) structure around 15 GPa in the anti-ferromagnetic (AFM) phase as well as in the paramagnetic (PM) insulating state which occurs above the Néel temperature ( $T_N$ ). This transition is relevant to interpreting the optical anomalies observed in the absorption spectrum of ruby under pressure. We have modeled the structural properties of the PM state using a Landau-like expansion of the magnetostriction energy. This treatment correctly describes the structural anomalies across  $T_N$  in the corundum phase and indicates that the AFM and PM insulating states should have distinct compressive behaviors.

71.15.-m, 61.50.Ks, 75.30.Kz, 62.50.+p

Oxides of the 3d transition metals are a fascinating class of materials with amazingly diverse physical properties. They have been a subject of intensive experimental and theoretical studies for many years [1–4]. A wide variety of computational techniques — density-functional theory with linear augmented plane wave method [2,5], non-periodic embedded cluster approach [6,7], periodic unrestricted Hartree-Fock method [8,9] — have been used to perform *ab initio* calculations of these compounds. In this paper we report a successful application of the first principles pseudo-potential plane-wave (PPPW) approach [10] to compute structural properties of and predict a pressure induced structural transition in chromia ( $\text{Cr}_2\text{O}_3$ ), a typical anti-ferromagnetic insulator in this class of materials. There were a few experimental papers on chromia [11–14] and only one *ab initio* calculation [9]. The periodic unrestricted LCAO Hartree – Fock method was used [9] to calculate crystal parameters and elastic properties, as well as electronic structure of  $\text{Cr}_2\text{O}_3$ . Their results are in a good agreement with experimental data. The advantage of the PPPW approach is in the simplicity of the plane-wave basis set, which makes it easy to calculate ionic forces and lattice stresses. This allowed us to optimize dynamically the cell structure of chromia under pressure [15] for various magnetic states.

Our motivation to study  $\text{Cr}_2\text{O}_3$  is related to the high pressure behavior of ruby, i.e.  $\text{Al}_{2(1-x)}\text{Cr}_{2x}\text{O}_3$  ( $x < 0.05$ ). The pressure dependence of the fluorescence lines in ruby is widely used to determine pressure (the so-called ruby scale) in diamond-anvil-cell experiments. Alumina ( $\text{Al}_2\text{O}_3$ ) and chromia exist in the corundum phase and form a completely isomorphous alloy system. Alumina has been shown to undergo a structural phase transition to the  $\text{Rh}_2\text{O}_3$  (II) phase around 80-100 GPa [16–18]. A recent theoretical study [19] of the effect of this structural transition on the optical spectrum of ruby indicated that the neighborhood of the chromium site, a *color center*,

might be undergoing a severe distortion around 30 GPa. This hypothesis is suggested by the behavior of the optical absorption lines which display a small discontinuity at 30 GPa and resemble more closely the transitions predicted in the high pressure  $\text{Rh}_2\text{O}_3$  (II) phase beyond 30 GPa than those in the corundum phase. It was then anticipated that the cause of this distortion could be a similar phase transformation at lower pressures ( $< 30$  GPa) in chromia, the other end member of the alloy. At the moment there is no convincing experimental evidence for a phase transformation in  $\text{Cr}_2\text{O}_3$  in this pressure range [20]. However, this may be due to the fact that the  $\text{Rh}_2\text{O}_3$  (II) phase has an X-ray diffraction pattern similar to corundum's [16], which makes it difficult to observe.

In this paper we investigate this pressure induced transformation in chromia. However another interesting question arises: at room temperature chromia undergoes a change in magnetic phase under pressure. Its Néel temperature is  $T_N = 308$  K [21], with a pressure dependence of  $\partial T_N / \partial P = -16$  K/GPa [22]. The paramagnetic (PM) state above  $T_N$  is also insulating; therefore, the effect of the magnetic transition on the structural properties are not expected to be dramatic. Nevertheless, structural anomalies around the Néel temperature are well known [23,24] and a realistic prediction of a possible phase transition above 0.5 GPa should be carried out in the PM insulating phase with randomly oriented spins. Here we investigate from first principles this structural transition in the AFM, and in a hypothetical ferromagnetic (FM) phases. The structural properties of PM insulating state is then explored in relation to those of the AFM and FM phases using a phenomenological approach based on a Landau-like expansion of the magnetostriction energy. The predicted structural differences of this phase with respect to the AFM phase correlate well with the anomalies

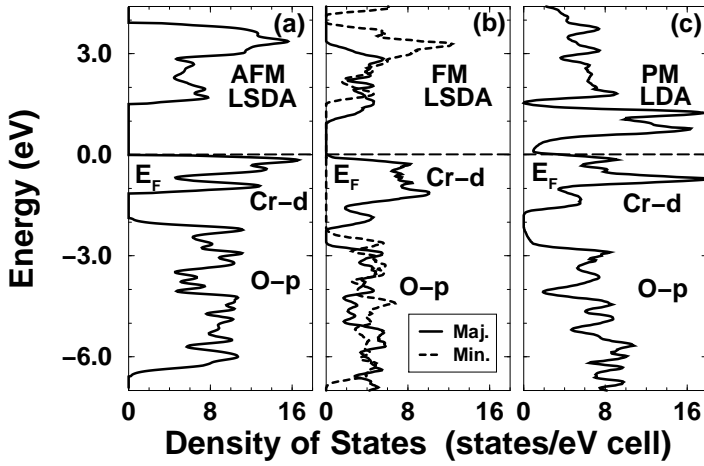


FIG. 1. Calculated DOS for various magnetic phases of  $\text{Cr}_2\text{O}_3$  in the corundum structure.

observed around the Néel transition and are very different from those of the PM metallic phase predicted by a standard LDA calculation.

The crystal structure of  $\text{Cr}_2\text{O}_3$  at ambient conditions is corundum-like. It can be described as a hexagonal closed packed array of oxygens with two thirds of the octahedral sites filled with chromium atoms. The unit cell is rhombohedral and contains two formula units. In  $\text{Cr}_2\text{O}_3$  each chromium is left with three  $d$ -electrons, losing the other three to oxygens. The predominantly octahedral crystal field splits  $d$ -orbitals into (approximately) a  $t_{2g}$ -like triplet and an  $e_g$ -like doublet. The lower triplet accommodates three electrons. The  $\text{Cr}^{3+}$  local magnetic moment is  $2.76\mu_B$ , [21] close to the spin only value of  $3\mu_B$ . The moments lie parallel to the  $c$ -axis, and are arranged in ferromagnetic layers perpendicular to the  $c$ -axis. The layers alternate up and down along the  $c$ -axis. In the insulating phase above  $T_N$  chromia has randomly oriented spins.

To investigate the effect of magnetism on the structural properties we have performed three distinct calculations: 1) a standard *spin-polarized* LSDA calculation [25] in the AFM phase of  $\text{Cr}_2\text{O}_3$  in the corundum structure; 2) same-type calculation in the FM phase, with the net magnetic moment of  $3\mu_B$  per  $\text{Cr}$  atom; 3) a standard *non-spin-polarized* LDA calculation in a PM phase. In all cases the lattice and internal degrees of freedom were dynamically relaxed under pressure [15]. The zero-pressure structures obtained correspond to various local minima of the LSD functional.

The ground state at  $T = 0$  K is the AFM state with a band gap of  $\approx 1.5$  eV (Fig. 1-a) and a local magnetic moment of  $3\mu_B$  on chromium atoms (from straight band occupations). The overall band structure compares well with photo-emission data [29,30]. Namely, the  $\text{O}_{2p}$  and  $\text{Cr}_{3d}$  band widths of 5 eV and 1 eV respectively, and  $\text{O}_{2p}$ - $\text{Cr}_{3d}$  band centers separation of 4 eV are in a good agreement with experimental values. However, as expected,

TABLE I. Zero pressure structural parameters of chromia in the corundum structure (rhombohedral unit cell): lattice constant  $a_0$  (Å) and rhombohedral angle  $\alpha$  (deg), internal atomic coordinates  $u(\text{Cr})$  and  $u(\text{O})$ , bulk modulus  $B_0$  (GPa) and its pressure derivative  $B'_0$ .

	AFM LSDA	FM LSDA	PM LDA	Experiment	
$a_0$	5.366	5.308	5.688	$5.362^c$	$5.350^d$
$\alpha$	55.17	56.14	47.23	$55.108^c$	$55.128^d$
$u(\text{Cr})$	0.347	0.351	0.337	$0.3475^c$	$0.3477^d$
$u(\text{O})$	0.557	0.550	0.583	$0.556^c$	$0.555^d$
$B_0^a$	$251 \pm 6$	$215 \pm 5$	$300 \pm 8$	$238 \pm 4^d$	$222 \pm 2^f$
$B_0^b$	$261 \pm 2$	$211 \pm 5$	$297 \pm 3$	$231 \pm 5^f$	
$B'_0^b$	2.59	2.73	4.24	$2.0 \pm 1.1^f$	

<sup>a</sup>Second order finite strain equation of state (FSEoS) ( $B'_0 \equiv 4$ ). We used our data up to 15 GPa for this fitting.

<sup>b</sup>Third order FSEoS was used with  $B'_0$  as free parameter. We include pressures up to 140 GPa to get a correct value of  $B'_0$ , while in Ref. [12] the pressure range was not sufficient for a confident determination of  $B'_0$ .

<sup>c</sup>Ref. [11]

<sup>d</sup>Ref. [13]

<sup>f</sup>Ref. [12]

the band gap is underestimated with respect to the thermal gap of 3.3 eV [31]. Zero-pressure equilibrium structural parameters presented in Table I are also in good agreement with experimental data. The cohesive energy of  $E_{coh} = 6.1$  eV/atom compares well with  $E_{coh} = 5.55$  eV/atom from experiments. The FM state is found to be insulating as well with a band gap of  $\approx 0.9$  eV (Fig.1-b). After structural relaxation this state is only 35 meV/unit above the AFM ground state. Equilibrium lattice parameters (Table I) are quite different from those in the AFM state, indicating a substantial influence of the magnetic state on the structural properties. The standard paramagnetic *non-spin-polarized* LDA calculation stabilizes  $\text{Cr}_2\text{O}_3$  in a *metallic* phase (Fig.1-c), as expected, with structural properties considerably different from the observed ones (see Table I). This state is 2.25 eV/unit above the AFM ground state and cannot properly account for the structural transition under consideration.

Our description of the structural properties of the PM phase is based on the Landau-like expansion of the crystal deformation energy at a certain fixed pressure,  $E = \lambda_{ijkl}u_{ik}u_{jl} + \beta_{ijkl}u_{ik}M_{1j}M_{2l}$ . Here  $u_{ik}$  is a strain tensor,  $\mathbf{M}_1$ ,  $\mathbf{M}_2$  are the magnetization vectors of the two AFM sublattices, and  $\lambda$  and  $\beta$  are constant tensors. The first term represents pure elastic deformation, while the second describes the magnetostriction energy, i. e., the coupling of the magnetic and structural degrees of freedom. Deformations conserving the corundum structure symmetry allow only for  $U = u_{33}$ , uniaxial strain, and  $V = \sum u_{ii}$ , hydrostatic compression. We assume  $\mathbf{M}_1$ ,  $\mathbf{M}_2$  remain parallel to the  $z$ -axis. The above expression then simplifies to:  $E = \lambda_1 V^2 + \lambda_2 U^2 - \lambda_{12} VU + (\beta_1 V + \beta_2 U) \cdot M_{1z}M_{2z}$ . The equilibrium configurations are such that  $U = u_0 \cdot M_{1z}M_{2z}$ ,  $V = v_0 \cdot M_{1z}M_{2z}$ , where

$u_0$  and  $v_0$  depend on  $\lambda$  and  $\beta$ . For the AFM and FM phases  $M_{1z}M_{2z} = -1$  and  $M_{1z}M_{2z} = 1$  respectively. For the PM state the average product  $\langle M_{1z}M_{2z} \rangle_{PM} = 0$ . Therefore, the equilibrium lattice structural parameters of the PM phase are given by:  $U_{PM} = (U_{AFM} + U_{FM})/2$ ,  $V_{PM} = (V_{AFM} + V_{FM})/2$  where  $U_{AFM}$ ,  $U_{FM}$ ,  $V_{AFM}$ , and  $V_{FM}$  have been determined from first principles. A similar procedure can be adopted for dealing with the  $Rh_2O_3$  (II) phase. In this case, the deformation energy is expressed as:  $E = \sum \lambda_{\gamma\delta} u_{\gamma} u_{\delta} + \sum \beta_{\gamma} u_{\gamma} \cdot M_{1z}M_{2z}$ , where  $\gamma, \delta = xx, yy, zz$ .

The predicted properties of the AFM and PM insulating states compare as follows: a) the difference in zero pressure lattice parameters (in the hexagonal cell description) between them, are similar to the anomalies observed around  $T_N$ . Throughout the Néel transition (AFM to PM), the calculated  $\Delta a_H = +0.013\text{\AA}$  and  $\Delta c_H = -0.11\text{\AA}$  agree in sign and approximately in order of magnitude with experimental values of  $\Delta a_H = +0.006\text{\AA}$  and  $\Delta c_H = -0.018\text{\AA}$  [23]. We believe this is evidence of the satisfactory description of the PM insulating state. b) The calculated compressive behavior of our PM insulating state compares well with the experimental behavior under pressure above  $T_N$  [12], while our AFM calculation is in better agreement with the experiment of Lewis and Drickamer [11], which we suspect may have been carried out in the AFM phase.

A summary of experimental data and our results is presented in Fig. 2. In Ref. [11] a substantial decrease of the rhombohedral angle with pressure was found (hexagonal  $c$ -axis less compressive than  $a-b$  axes). In contrast, in Ref. [12] a slight increase in this angle was observed ( $c$ -axis more compressive than  $a-b$  axes). This discrepancy has been attributed to non-hydrostatic stresses in Ref. [11]. Our results suggest this discrepancy could be real if somehow in Ref. [11] chromia was kept in the AFM state. We predict here that the magnetic state affects noticeably the compressive behavior of chromia despite the insulating nature of both phases. Compression experiments well below and well above  $T_N$  could help to clarify this situation.

Now we deal with the structural transition. The high pressure  $Rh_2O_3$  (II) phase has  $Pbna$  space group with an orthorhombic unit cell containing 20 atoms (four  $Cr_2O_3$  units). This phase is structurally similar to the corundum structure and may be described as having a different stacking of similar octahedral layers with a periodicity which is twice that of the corundum along the ' $c$ ' direction [32]. In the corundum structure the  $CrO_6$  octahedra share three edges while in the  $Rh_2O_3$  (II) structure they share only two. The relative stability of these structures in both magnetic states is shown in Fig. 3-a. We predict the corundum to  $Rh_2O_3$  (II) transformation in chromia to take place at 14 GPa and 16 GPa in the AFM and in the PM insulating phases respectively, with fractional volume changes at the transition of  $\approx -2\%$ . This transition would also take place in the FM phase if it were somehow stabilized.

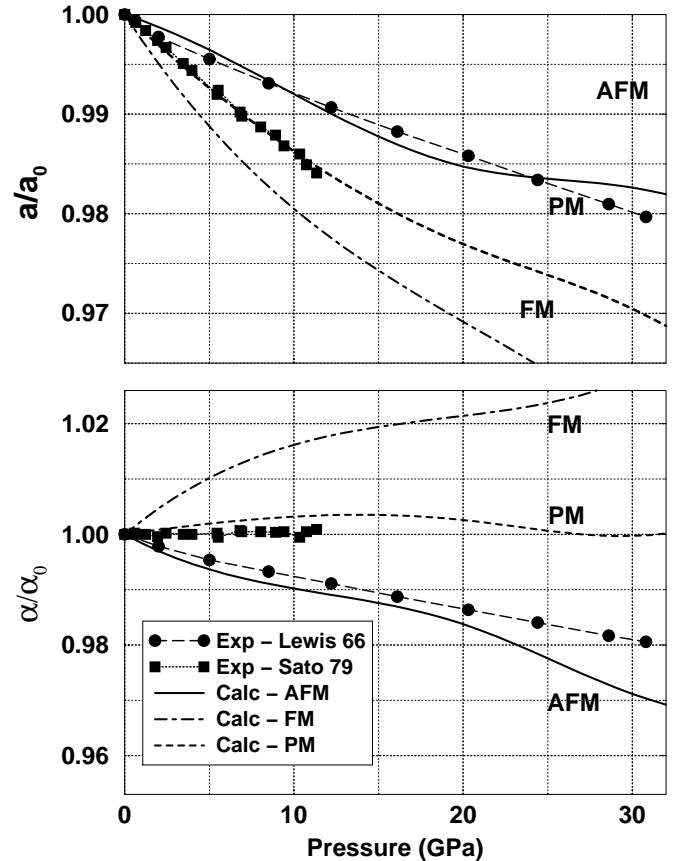


FIG. 2. Pressure dependence of the  $Cr_2O_3$  rhombohedral cell constant  $a$  and angle  $\alpha$ , calculated for AFM, FM and PM phases compared to experimental measurements from Ref. [11] (Lewis 66) and Ref. [12] (Sato79).

Fig. 3-b displays the average radius of the first coordination shell around chromium in AFM chromia and in ruby (from Ref. [19]). The average Cr-O bond-length in chromia increases across the corundum to  $Rh_2O_3$  (II) transition by an amount similar to that required to explain the optical anomalies in ruby under pressure, which can be explained by a decrease in crystal field splitting. This verifies that this presumable rearrangement could arise from a preference of chromia for the  $Rh_2O_3$  (II) phase above  $\approx 15$  GPa. The structural constraint imposed by the alumina host structure should naturally hinder the atomic rearrangement around the color centers until higher pressures, for instance 30 GPa.

These results should stimulate further experimental and theoretical work. The prediction of distinct compressive behaviors in chromia above and below  $T_N$  and the structural phase transformation near 15 GPa await experimental confirmations. The latter, if verified, makes ruby an interesting study case: an isomorphous alloy in which both end members undergo the same structural transition but at very different pressures. Intermediate compositions should undergo similar transitions at intermediate pressures. However, before the transformation

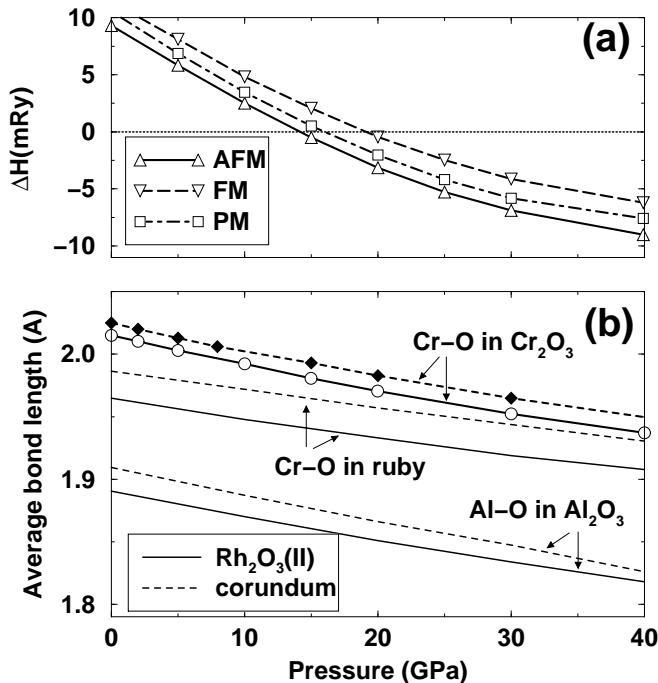


FIG. 3. (a) Pressure dependence of the enthalpy for  $\text{Rh}_2\text{O}_3$  (II) structure, relative to the corundum in AFM and PM phases; (b) Average radii of the first coordination shell around chromium in chromia and ruby [19], and aluminum in alumina [19].

manifests macroscopically it could be nucleating around one of the components, even in the impurity limit. The possibility of investigating this phenomenon in ruby by EXAFS or anomalous X-ray scattering is fascinating.

*Acknowledgments* - We thank Phil Allen and Stefano Baroni for helpful comments on the manuscript. This work was supported by the University of Minnesota MRSEC (AYuD), and NSF grant EAR-9973130 (RMW and WD).

[1] N. F. Mott, Proc. Phys. Soc. London, Ser. A **68**, 416 (1949); J. Hubbard, *ibid.* A **277**, 237 (1964); *ibid.* **5** 401 (1964); B. H. Brandow, Adv. Phys. **26**, 651 (1977).  
 [2] K. Terakura et al., Phys. Rev. Lett. **52**, 1830 (1984); Phys. Rev. B **30**, 4734 (1984).  
 [3] R. M. Wentzcovitch, W. Schulz, and P. B. Allen, Phys. Rev. Lett. **72**, 338 (1993); *ibid.* **73** (Comm.), 3043 (1994).  
 [4] S. P. Lewis, P. B. Allen, and T. Sasaki, Phys. Rev. B **55**, 10253 (1997).  
 [5] P. Dufek et al., Phys. Rev. B **49**, 10170 (1994).  
 [6] J. Casanovas and F. Illas, Phys. Rev. B **50**, 3789 (1994).  
 [7] J. A. Mejias and J. F. Sanz, J. Chem. Phys. **102**, 850 (1995).  
 [8] M.D. Towler et al., Phys. Rev. B **50**, 5041 (1994).

[9] M. Catti et al., J. Phys. Chem. Solids **57**, 1735 (1996).  
 [10] M. L. Cohen, Phys. Scr. T **1**, 5 (1982); W. E. Pickett, Comp. Phys. Rep. **9**, 115 (1989).  
 [11] G. K. Lewis, Jr. and H. G. Drickamer, J. Chem. Phys. **45**, 224 (1966).  
 [12] Y. Sato, and S. Akimoto, J. Appl. Phys. **50**, 5285 (1979).  
 [13] L. W. Finger, and R. M. Hazen, J. Appl. Phys. **51**, 5362 (1980).  
 [14] X. Li, L. Liu, and V. E. Henrich, Sol. St. Comm. **84**, 1103 (1992).  
 [15] R. M. Wentzcovitch, J. L. Martins, and G. D. Price, Phys. Rev. Lett. **70**, 3947 (1993).  
 [16] K. T. Thomson, R. M. Wentzcovitch, M. S. T. Bukowinski, Science **274**, 1880 (1996).  
 [17] H. Cynn et al., Am. Mineral. **75**, 439 (1990); F. C. Marton and R. E. Cohen, Am. Mineral. **79**, 789 (1994).  
 [18] N. Funamori and R. Jeanloz, Science **278**, 1109 (1997).  
 [19] W. Duan et al., Phys. Rev. Lett., **81**, 3267 (1998).  
 [20] L.-G. Liu and W. A. Bassett, *Elements, Oxides, and Silicates: High Pressure Phases with Implications for the Earth's Interior* (Oxford Press, New York, 1986), p. 126.  
 [21] L.M. Corliss et al., J. Appl. Phys. **36**, 1099 (1965).  
 [22] T. G. Worlton, R. M. Brugger, and R. B. Bennion, J. Phys. Chem. Solids **29**, 435 (1968).  
 [23] H.L. Alberts, J.C.A. Boeyens, J. Mag. Mat. **2**, 327 (1976). Lattice parameters in the PM phase were measured up to T=400 K and extrapolated to T=0 K.  
 [24] S.Greenwald, Nature **177**, 286 (1956).  
 [25] The norm-conserving Troullier-Martins [26] pseudopotentials (cutoff radii in a.u.:  $O r_s = r_p = 1.45$ ;  $Cr r_s = r_p = 2.5$ ,  $r_d = 1.75$ ) with partial core correction [27] (pseudocore radius for  $Cr$ :  $r_c = 1.6$ ) in the plane-wave basis set were used [10]. The plane-wave energy cutoffs were 70 Ry for wave functions and 280 Ry for charge densities and potentials. Brillouin-zone summations were performed over two k-points in the irreducible wedge. We used Ceperley and Alder LSDA exchange-correlation potential parameterized by Perdew and Zunger [28].  
 [26] N. Troullier and M. L. Martins, Phys. Rev. B **43**, 1993 (1991).  
 [27] S.G. Louie, S. Froyen, and M.L. Cohen, Phys. Rev. B **26**, 1738 (1982).  
 [28] D. M. Ceperley, and B. J. Alder, Phys. Rev. Lett. **45**, 566 (1980); J. Perdew and A. Zunger, Phys. Rev. B **23**, 5048 (1981).  
 [29] G. K. Wertheim, H. J. Guggenheim, and S. Hüfner, Phys. Rev. Lett. **30**, 1050 (1973).  
 [30] D. E. Eastman and J. L. Freeouf, Phys. Rev. Lett. **34**, 395 (1975).  
 [31] J. A. Crawford and R. W. Vest, J. Appl. Phys. **35**, 2413 (1964).  
 [32] R. D. Shannon, and C. T. Prewitt, J. Solid State Chem. **2**, 134 (1970).